Geophys. J. Int. (2002) **150,** 467–482

Excitation Sompi method and its application to an analysis of the Earth's polar motion

Yukiko Yokoyama

Dept. Biosphere–Geosphere System Science, Okayama University of Science, 1-1 *Ridaicho, Okayama* 700-0005, *Japan. E-mail: yokoyama@big.ons.ac.jp*

Accepted 2002 February 18. Received 2002 January 15; in original form 2001 April 30

SUMMARY

We present a practical excitation Sompi method. The excitation Sompi method is a non-stationary time-series method developed for the analysis of physical phenomena that obey time-invariant linear processes. Hence, the model is a discrete form of an inhomogeneous linear differential equation. In contrast with previous methods, this method has three advantages: (1) the method estimates both the eigen coefficients of the dynamic system and the excitation sequence almost simultaneously; (2) the excitation sequence is without statistical constraints and can have a wide variety of characteristics; (3) the parameter estimation method is constructed to be robust for practical use: parameters with small error can be estimated even if the assumed model conditions are not fully satisfied.

We demonstrate the usefulness of the present method by applying it to the analysis of the Earth's polar motion. We analysed SPACE95 data from 1976 to 1996 with a three-day sampling interval. As a result, a real eigenfrequency between 2.33×10^{-3} and 2.39×10^{-3} cpd was estimated. This is slightly larger than the previously estimated value of 2.30×10^{-3}cpd. Because the previous methods, which lack these three advantages, tend to estimate biased parameters, our result is thought to be closer to the true value. On the other hand, Q, which was estimated to be from several tens to a thousand by previous methods, was estimated by the present method to fall in a range from 90 to 346. Using the present method, we thus succeeded in estimating a less biased real eigenfrequency and in restricting the range of Q. This will also be a powerful method for the analysis of other kinds of physical phenomena that obey linear time-invariant dynamic processes.

Key words: Chandler wobble, Earth rotation, excitation Sompi method, inhomogeneous AR model, polar motion, time-series analysis.

1 INTRODUCTION

There are many geophysical phenomena that obey a linear deterministic process (e.g. Fowler 1990). Their physical rules can generally be described by an inhomogeneous linear differential equation:

$$c_0 \frac{d^p \mathbf{x}(t)}{dt^p} + c_1 \frac{d^{p-1} \mathbf{x}(t)}{dt^{p-1}} + \cdots + c_p \mathbf{x}(t) = \mathbf{u}(t). \quad (1)$$

In eq. (1), the coefficients c_j indicate characteristics of the dynamic system and can be rewritten as complex eigenfrequencies. The term $\mathbf{u}(t)$ on the right-hand side represents an external force or excitation. When the excitation acts on the system, the system responds according to its characteristic values and generates a displacement $\mathbf{x}(t)$. To clarify the physical mechanisms of the system, we need to analyse the observable quantity $\mathbf{x}(t)$ and estimate both c_j values and $\mathbf{u}(t)$.

In such an analysis, the time-series data $\mathbf{x}(t)$ are generally non-stationary. When the coefficients c_j temporally change, the system is time-variant and the phenomenon is essentially non-stationary. The phenomenon also becomes non-stationary when the system is time-invariant and a general excitation exists. Accordingly, the techniques of non-stationary time-series analysis are necessary to estimate the c_j values and $\mathbf{u}(t)$.

With a view to clarifying the physical mechanisms, we classified the techniques for non-stationary time-series analysis into three categories. Techniques of the first category do not conform to the dynamic eq. (1). Those of the second and the third categories conform to the equation, but techniques in the second category are suitable to a time-variant system while those in the third category are suitable to a time-invariant system.

Wavelet analysis is a popular technique belonging to the first category (e.g. Chui 1992). The analysis transfers data from physical space to the space constituted with wavelets. If the proper analyzing wavelet is selected, the transferred data describe the data features well. However, the transfer does not relate directly to a physical process. Hence, the results are preliminary and do not have a physical meaning directly.

Techniques of the second category usually require models. Most of these models place restrictions on $\mathbf{u}(t)$, because it is impossible to estimate both c_j values and $\mathbf{u}(t)$ without any *a priori* information. Windowed Fourier analysis is a popular method for modelling a time-variant system (e.g. Oppenheim & Schafer 1999). This analysis tacitly assume the slow temporal change of the system and no excitation because Fourier analysis is a stationary time-series analysis method based on time-invariant system without excitation. An time-varying autoregressive (AR) model and an autoregressive moving average (ARMA) model have a similar physical meaning, but white or coloured noise excitation is assumed (Dembo & Zeitouni 1988; Grenier & Omnes-Chevalier 1988; Kanai *et al.* 1992). Analysis by a Kalman filter also has a similar physical meaning, but the system characteristics can change quickly (Kalman & Bucy 1961; Grewal & Andrews 1993).

Techniques of the third category also use models with special assumptions about the excitation. For example, the ARMA model assumes a coloured noise excitation (e.g. Kay & Marple 1981), and the autoregressive integrated moving average (ARIMA) model assumes an integrated coloured noise excitation (Box & Pierce 1970).

Because of such special assumptions about the excitation, the preexisting methods can be applied to limited kinds of data. In contrast, we have developed a new method that can be applied more broadly (Yokoyama *et al.* 1997, 1999, 2000, hereafter papers I, II and III, respectively). We first described a dynamic equation for a time-invariant system with a discrete form as an inhomogeneous autoregressive (IAR) model. This model can express general phenomena generated by time-invariant linear systems. Then we developed the excitation Sompi method, which is one of the parameter estimation methods of the IAR model. This method was designed to keep the generality of the IAR model as far as possible. While the pre-existing methods impose tight conditions on the excitation, conditions required by our method are flexible and moderate. Hence, we can express a variety of excitation sequences.

In the first half of this paper, we propose an extended and improved version of the excitation Sompi method. In paper I, we presented a basic model constituting the fundamental part and its parameter estimation method. While the basic model was formulated for single-component data, we extend the model in this paper to two-component data. This widens possible applications of the method. The upper-layer model of the basic model, the model group, was described in papers II and III. We improve on the criteria and method for parameter estimation of the model group in this paper, enabling us to use the method even when its assumptions are not fully satisfied. With these extensions and improvements, the method is complete and ready for practical use.

In the second half of this paper, we apply the present method to an analysis of the Earth's polar motion from 1976 to 1996. Polar motion is a two-component motion and obeys a first-order linear differential equation (e.g. Lambeck 1980; Moritz & Mueller 1988). The system of polar motion is assumed to have time-invariant physical characteristics on the timescale spanned by the data. Although the causes of the polar motion excitation have not been clarified in detail, torques from the atmosphere, the ocean, earthquakes, and the core–mantle coupling are thought to be candidates (e.g. Lambeck 1980). Hence, the excitation can be a mixture of different sources and has a wide variety of characteristics. Such a phenomenon that obeys a time-invariant linear process and that has a compound excitation sequence is appropriate for a demonstration of the excitation Sompi method.

There are many previous studies of polar motion, and the major results of these studies are summarized in Table 1. Because the polar motion system is mostly time-invariant, as mentioned above, few analyses used a time-variant model (Kosek & Kolaczek 1997). Analysis methods using time-invariant models are sorted into three groups. Methods of the first group estimate only a real eigenfrequency and Q, assuming a stationary polar motion (Jeffreys 1968; Chao 1983; Wilson & Vincente 1990). Those of the second group estimate an excitation sequence using a given real eigenfrequency and Q (Preisig 1992; Chao 1993; Rio & Cazenave 1994). Methods in the last group impose tight restrictions on the excitation sequence and estimate a real eigenfrequency and Q (Ooe 1978; Wilson & Vincente 1980; Furuya & Chao 1996; Kuehne *et al.* 1996).

Parameters estimated by such analyses tend to include a large bias. The assumption of methods of the first group is incompatible with the character of the actual data: polar motion data is non-stationary because of excitations. The neglect of the effect of the excitation tends to generate a bias in the estimated real eigenfrequency and Q. When methods of the second group are used, the excitation sequence can be seriously misestimated, depending on the given real eigenfrequency and Q. In methods of the last group, the imposed restrictions on the excitation sequence are generally not satisfied by the actual excitation sequence. The difference between the assumptions and the actuality usually induces a bias in the estimated real eigenfrequency and Q. In contrast with these pre-existing methods, the method proposed in this paper does not have such disadvantages. Hence, it enables a real eigenfrequency, Q, and excitation sequence with smaller bias to be estimated.

Table 1. Analysis results of polar motion by preexisting and the present methods.

System	Stationary or Non-stationary	Method or model	Real eigenfrequency (cpd)	Q	Excitation function	Reference
Time-variant	Non-stationary	FT-BPF	[$(2.083–3.125) \times 10^{-3}$]	[Infinity]	Fully-estimated	Kosek & Kolaczek 1997
Time-invariant	Stationary	Maximum likelihood	2.304×10^{-3}	61 (37, 185)	[White noise]	Jeffreys 1968
		AR method	$(2.209–2.460) \times 10^{-3}$	(–1930, 711)	[None]	Chao 1983
		AR model	2.311×10^{-3}	179 (74, 789)	[White noise]	Wilson & Vincente 1990
	Non-stationary	Kalman filter	[2.309×10^{-3}]	[170]	Fully estimated	Preisig 1992
		Dynamic equation	[2.299×10^{-3}]	[100]	Fully estimated	Chao 1993
		Dynamic equation	[2.299×10^{-3}]	[100]	Fully estimated	Rio & Cazenave 1994
		ARMA model	2.301×10^{-3}	96 (50, 300)	[Colored noise]	Ooe 1978
		ARMA model	2.310×10^{-3}	170 (47, 1000)	[Colored noise]	Wilson & Vincente 1980
		Monte Carlo	2.306×10^{-3}	49 (35, 100)	[Atmospheric data]	Furuya & Chao 1996
		Monte Carlo	2.275×10^{-3}	72 (30, 500)	[Atmospheric data]	Kuehne *et al.* 1996
		Excitation Sompi	2.362×10^{-3}	143 (90, 346)	Fully estimated	This paper

[] indicates assumed value/character.

In the next section, we present the excitation Sompi method including both the established and newly developed parts. In Section 3, we perform some synthetic tests of the method to confirm its capabilities, and then we analyse a series of polar motion data in Section 4. In Section 5, we summarize and discuss the results.

2 EXCITATION SOMPI METHOD

We present the excitation Sompi method in its entirely in this section. The fundamental part of the method has already been established in papers I, II and III, but we extend and improve the method here. The newly developed elements are as follows:

(1) We rewrote the formulae of the method, which were written for single-component data in paper I, for the analysis of two-component data.

(2) In papers II and III, we used three criteria for parameter estimation: (i) minimize the root mean square (rms) error of the input sequence; (ii) minimize scattering of estimated frequencies of the model group; and (iii) minimize the rms error of the output sequence. In this paper, we replaced the second criterion with criterion (ii′): adopt frequencies smaller than a reciprocal number of the initially given AR order and minimize their scattering; and we deleted the third criterion.

(3) We changed the parameter estimation procedure as required by the new criterion (ii′).

We present the method with detailed explanations of the new elements in the following subsections.

2.1 Model

We consider data with two orthogonal components. To treat the components simultaneously, we define complex discrete data $\tilde{x}_n$, whose real part is the first component of the data and whose imaginary part is the second. Then the two-component IAR model is written with complex AR coefficients $\tilde{a}_j$, AR order p, and complex excitation $\tilde{u}_n$ as

$$\sum_{j=0}^{p} \tilde{a}_j \tilde{x}_{n-j} = \tilde{u}_n. \tag{2}$$

This is a discrete model of the two-component inhomogeneous linear differential equation (1).

Considering observation noise, we describe observable data $\tilde{y}_n$ as

$$\tilde{y}_n = \tilde{x}_n + \tilde{\varepsilon}_n. \tag{3}$$

In eq. (3), complex noise $\tilde{\varepsilon}_n$ is assumed to be a random sequence with zero mean and variance σ^2.

To take into account *a priori* information about the excitation $\tilde{u}_n$, and make estimation possible, we assume that $\tilde{u}_n$ is expanded with a proper set of basis $\tilde{\varphi}_{n,j}$ with complex coefficient $\tilde{\beta}_j$ and degree q:

$$\tilde{u}_n = \sum_{j=1}^{q} \tilde{\beta}_j \tilde{\varphi}_{n,j}. \tag{4}$$

The character of the sequence $\tilde{u}_n$ can be controlled by changing the basis set $\tilde{\varphi}_{n,j}$. For example, a stochastic process can be approximately described by a narrow width basis, and a deterministic process can be described by a basis created from a proper waveform and width. An excitation of mixed process can be described by combining the different kinds of basis sets. When proper amplitudes $\tilde{\beta}_j$ are supplied, a stationary excitation can be described. An event-based excitation can also be expressed by assigning a zero amplitude to some $\tilde{\beta}_j$.

Eqs (2), (3) and (4) constitute the model of the two-component excitation Sompi method.

2.2 Policy and criteria

We use the two criteria described above. The first criterion (i) was presented in paper I. It is based on a sense of achieving a good fit between the data and the model. The fit is evaluated not in data space but in excitation space. Such an evaluation is used by methods that take into account observation noise, such as the Pisarenko and extended Prony methods (e.g. Kay & Marple 1981). The other criterion (ii′) is an improved version of criterion (ii) presented in paper III. It was derived as is described below.

A model world based on assumptions is different from the actual world. For example, while white noise is assumed in the model, the actual noise may have colour and may include pulsations. Nonlinear signal may be contaminated while the system is assumed to be linear. Furthermore, the assumed basis set is not the true basis set because the true excitation is unknown.

When such differences cannot be neglected, it is not possible to use the classical least-squares method for parameter estimation. This problem has been studied, and some new techniques have been presented. One such technique is robust estimation (Huber 1981; Kassam & Poor 1985). This method considers the case when errors of the least-squares method do not obey a Gaussian distribution. Another technique is the H_∞ filter, which extends the Kalman filter and considers non-white noise (Nagpal & Khargonechker 1991; Shaked & Theodor 1992). As in the previous studies, we take into account differences from the assumptions, which we shall call model selection error.

Because the estimation error does not necessarily obey a particular stochastic distribution, in general we cannot avoid estimation bias caused by model selection error. Hence, we select a way to diminish estimation error rather than to diminish the bias. An estimated physical quantity with sufficiently small error is enough for our needs even if the small error is biased.

The estimation error becomes small when the initially given AR order p becomes sufficiently larger than the true AR order p_0 (paper III). Because the model selection error and noise are divided and absorbed by the given p parameters, parameter estimation errors become small when the number of given parameters increases. Accordingly, we can estimate parameters close to true values if we supply a large number of parameters.

We proved the relation between the size of the error and the number of given parameters in paper III, and derived criterion (ii) for AR order estimation. When the initially given AR order increases, the values of the estimated parameters that are close to true values gradually approach true values. When the number of parameters becomes sufficiently large, the estimated parameter values will not change any more because they are already close enough to true values. In other words, the parameter values close to true values do not change against a high initially given AR order. Thus, parameters with small scattering in response to a change in the initially given AR order are preferred. This is what the original criterion (ii) implies.

Although the criterion is necessary for the selection of preferred parameters, it is not sufficient. It is still possible to select parameters, such as Nyquist frequency, originating from noise or model selection error. Thus, we need another constraint to exclude such parameters. We present such a constraint in the new criterion (ii′).

In the appendix to paper III, it is proved that frequencies originating in noise or model selection error are expected to be larger than the order of $1/(p-p_0)\Delta t$, where Δt indicates the sampling interval. Thus, we regard the frequencies larger than $1/(p-p_0)\Delta t$ as of noise or model error origin. Frequencies smaller than $1/(p-p_0)\Delta t$ and with small scattering are regarded as of signal origin. In the actual analysis, we take large values of p and use $1/p\Delta t$ instead of $1/(p-p_0)\Delta t$ because we do not know p_0. Thus, we have criterion (ii′). With this criterion, we cannot extract signal frequencies larger than $1/p\Delta t$. However, if we know the rough frequency range of the signal, we can extract such signals by changing Δt.

When we use this criterion, the selected frequencies correspond to those estimated, and their number equals the estimated AR order. The estimation of the frequencies is equivalent to the estimation of the AR parameters, so it is approximately equivalent to the estimation of $\tilde{u}_n$ in eq. (2). Accordingly, we can estimate all the parameters with criterion (ii′), and criterion (iii) is not necessary any more. Detailed procedures for using criterion (ii′) are described in subsections 2.4 and 2.5.

2.3 Estimation of the basic model parameters

The model of the excitation Sompi method written in eqs (2), (3) and (4) has four kinds of independent parameters, $\tilde{a}_j, p\ \tilde{\beta}_j$ and $\tilde{\varphi}_{n,j}$. The parameter q is not independent because it is the degree of basis set $\tilde{\varphi}_{n,j}$. Because the simultaneous estimation of all parameters is difficult, we first prepare proper candidate sets $\tilde{\varphi}_{n,j}$, and then we select a good choice from them. For each candidate set $\tilde{\varphi}_{n,j}$, we prepare candidate models with different initially given AR orders p. We call a group of candidate models for a given set $\tilde{\varphi}_{n,j}$ a model group, and we call each model with an initially given AR order a basic model. In other words, a set of candidate models is composed of model groups, and each model group is composed of basic models.

Parameters of the basic model, $\tilde{a}_j$ and $\tilde{\beta}_j$, are estimated simultaneously using criterion (i). This parameter estimation method was suggested in paper I, and we here extend the method from a single component to two components.

The rms error in the excitation space is defined as follows:

$$S=\frac{1}{N-p}\sum_{n=p}^{N-1}\left|\sum_{j=0}^{p}\tilde{a}_j(\tilde{y}_{n-j}-\tilde{\varepsilon}_{n-j})-\sum_{j=1}^{q}\tilde{\beta}_j\tilde{\varepsilon}_{n,j}\right|^2. \tag{5}$$

Minimizing the rms error, we have

$$\begin{bmatrix}\tilde{\boldsymbol{P}} & -\tilde{\boldsymbol{\Phi}}\\ -\tilde{\boldsymbol{\Phi}}^* & \tilde{\boldsymbol{\Psi}}\end{bmatrix}\begin{bmatrix}\tilde{\boldsymbol{A}}\\ \tilde{\boldsymbol{B}}\end{bmatrix}=\lambda\begin{bmatrix}\tilde{\boldsymbol{A}}\\ 0\end{bmatrix}, \tag{6}$$

where

$$\tilde{\boldsymbol{P}}=\frac{1}{N-p}\begin{bmatrix}\sum_{n=p}^{N-1}\tilde{y}_n\tilde{y}_n^* & \cdots & \sum_{n=p}^{N-1}\tilde{y}_{n-p}\tilde{y}_n^*\\ \vdots & \ddots & \vdots\\ \sum_{n=p}^{N-1}\tilde{y}_n\tilde{y}_{n-p}^* & \cdots & \sum_{n=p}^{N-1}\tilde{y}_{n-p}\tilde{y}_{n-p}^*\end{bmatrix}, \tag{7}$$

$$\tilde{\boldsymbol{\Phi}}=\frac{1}{N-p}\begin{bmatrix}\sum_{n=p}^{N-1}\tilde{y}_n\tilde{\varphi}_{n,1}^* & \cdots & \sum_{n=p}^{N-1}\tilde{y}_n\tilde{\varphi}_{n,q}^*\\ \vdots & \ddots & \vdots\\ \sum_{n=p}^{N-1}\tilde{y}_{n-p}\tilde{\varphi}_{n,1}^* & \cdots & \sum_{n=p}^{N-1}\tilde{y}_{n-p}\tilde{\varphi}_{n,q}^*\end{bmatrix}, \tag{8}$$

$$\tilde{\boldsymbol{\Psi}}=\frac{1}{N-p}\begin{bmatrix}\sum_{n=p}^{N-1}\tilde{\varphi}_{n,1}\tilde{\varphi}_{n,1}^* & \cdots & \sum_{n=p}^{N-1}\tilde{\varphi}_{n,1}\tilde{\varphi}_{n,q}^*\\ \vdots & \ddots & \vdots\\ \sum_{n=p}^{N-1}\tilde{\varphi}_{n,q}\tilde{\varphi}_{n,1}^* & \cdots & \sum_{n=p}^{N-1}\tilde{\varphi}_{n,q}\tilde{\varphi}_{n,q}^*\end{bmatrix}, \tag{9}$$

$$\tilde{\mathbf{A}}=\begin{bmatrix}\tilde{a}_0\\ \vdots\\ \tilde{a}_p\end{bmatrix}, \tag{10}$$

and

$$\tilde{\mathbf{B}}=\begin{bmatrix}\tilde{\beta}_1\\ \vdots\\ \tilde{\beta}_q\end{bmatrix}, \tag{11}$$

Eq. (6) is the eigen equation, which is the fundamental equation of the basic model. Here the variance of the noise is substituted by the eigenvalue. The left matrix on the left-hand side of eq. (6) is a Hermitian matrix in the two-component case, while it is a real symmetric matrix in the single-component case.

Eliminating the vector from eq. (6), we have

$$(\tilde{\mathbf{P}}-\tilde{\boldsymbol{\Phi}}^*\tilde{\boldsymbol{\Psi}}^{-1}\tilde{\boldsymbol{\Phi}})\tilde{\mathbf{A}}=\lambda\tilde{\mathbf{A}}, \tag{12}$$

Solving eq. (12), we have the eigenvector $\tilde{\mathbf{A}}$ that corresponds to the minimum eigenvalue. Then the roots are estimated from

$$\tilde{\mathbf{A}}^T\tilde{\mathbf{Z}}=0, \tag{13}$$

where

$$\tilde{\mathbf{Z}}=\begin{bmatrix}\tilde{z}^0\\ \vdots\\ \tilde{z}^{-p}\end{bmatrix} \tag{14}$$

and

$$\tilde{z}=e^{2\pi i\tilde{f}} \tag{15}$$

In eq. (15), indicates a complex eigenfrequency.

Because the coefficients in eq. (13) are complex, the equation has p roots. In the single-component case, the coefficients are real and the equation has $p/2$ roots of complex conjugate pairs when p is even and $(p-1)/2$ roots of complex conjugate pairs and a real root when p is odd.

2.4 Estimation of the model group parameters

Parameters of the model group, the AR order and AR parameters $\tilde{a}_j$, are estimated using criterion (ii′). This estimation procedure has four steps. The outline of the procedure and the details of the first step are mostly the same as described in papers II and III. However, we change the details of the other steps in this paper.

The first step is the determination of the range of the initially given AR order p. While the initially given AR order should be larger than the true AR order as mentioned above, the true AR order is unknown. Hence, we set the initially given AR order to $p=1,2,\ldots,P$, with large P. That is, we prepare P basic models.

The second step is the estimation of candidate eigenfrequencies. We first estimate the parameters of each basic model, and then transfer the estimated AR parameters to eigenfrequencies with eq. (13).

Next, we discard frequencies higher than $1/p$ because they may be of noise or model selection error origin.

The third step is the estimation of AR order. Associating each basic model with the initially given AR order p, we sort the remaining frequencies in ascending order and number them $\tilde{f}_p^{(1)}, \tilde{f}_p^{(2)}, \ldots, \tilde{f}_p^{(K)}$. Then we determine the rough region $p = P_1, P_1+1, \ldots, P_2$ where the frequencies seem to be stable against p, and calculate their standard deviation $\sigma_f^{(k)}$ as

$$\sigma_f^{(k)} = \sqrt{\frac{1}{P_2 - P_1 + 1} \sum_{p=P_1}^{P_2} \left| \tilde{f}_p^{(k)} - \bar{\tilde{f}}^{(k)} \right|^2 w_p}. \tag{16}$$

In eq. (16), the mean frequency is defined as

$$\bar{\tilde{f}}^{(k)} = \frac{1}{P_2 - P_1 + 1} \sum_{p=P_1}^{P_2} \tilde{f}_p^{(k)} w_p, \tag{17}$$

and w_p is a weighting factor. In this step, only a rough estimation of $\sigma_f^{(k)}$ is sufficient, so we set all the weighting factors to unity. Such preliminary estimation diminishes a computational load of determining the weighting factor for all the remaining frequencies. When $\sigma_f^{(k)}$ is small enough, it indicates the stability of the eigenfrequency $\tilde{f}^{(k)}$, and the stability implies closeness of the estimated value to the true value. Then we estimate the AR order as the number of stable frequencies.

In the last step, we estimate preferred eigen frequencies. We recalculate the mean frequency in eq. (17) supplying the weighting factors from M-estimates (e.g. Huber 1981). We introduce M-estimates here because of the inhomogeneous distribution of the candidate frequencies. This estimation also excludes extremely biased values caused by the non-linear algorithm used by the root-finding problem in eq. (13). Strictly speaking, the meaning of the frequencies finally estimated is statistically unclear. However, this point can be neglected because the scattering of the candidate frequency is usually quite small.

In the practical calculation in the following sections, we use Tukey's biweight, which among various M-estimates has a gentle nature (Tukey 1974; Huber 1981). The ψ-function in this method is as follows:

$$\psi(x) = \begin{cases} x(1-x^2)^2 & for\ |x| \le 1 \\ 0 & otherwise. \end{cases} \tag{18}$$

When we use the above procedure, we can reduce the computational load in addition to diminishing the effect of noise and model selection error (Yokoyama *et al.* 2000). When we used the method in paper III, we needed to recover the output sequence and to calculate $P_2 - P_1 + 1$ times the rms error in the last step. However, we do not need to recover the output sequence in the present method. Hence, we can estimate the parameters with an extremely small computational load.

2.5 Selection of the basis set

Criterion (ii′) is also used to select the basis set. In paper II, we used criterion (iii) and directly estimated the basis set. However, we do not need to use direct estimation in the present method, because the model group parameters are hardly affected by the difference between the given and the true basis set. Hence, we adopt the candidate basis set that shows the smallest scattering of estimated frequencies. Then we adopt the associated AR order and eigenfrequencies.

2.6 Recovery of input and output sequences

Using the parameters estimated by the preceding steps, we finally recover input and output sequences. To make the calculation simpler, we first transfer the estimated eigenfrequencies $\bar{\tilde{f}}^{(k)}(k = 1, 2, \ldots, p)$ into the corresponding AR parameters $\tilde{a}'_j$ and recover the input sequence with

$$\tilde{u}_n = \sum_{j=0}^{p} \tilde{a}'_j \tilde{y}_{n-j}. \tag{19}$$

In this case, $\tilde{u}_n$ contains noise because $\tilde{y}_n$ is used instead of $\tilde{x}_n$. We can use a low-pass filter on $\tilde{u}_n$ and remove most noise as demonstrated in paper II if necessary. However, we do not use any filter here for simplicity.

The output sequence is recovered using the recovered $\tilde{u}_n$ as follows:

$$\tilde{x}_n = \begin{cases} \sum_{j=1}^{p} \tilde{C}_j \tilde{z}_j'^n - \sum_{j=1}^{p} \tilde{a}'_j \tilde{x}_{n-j} = \tilde{u}_n & \\ \qquad\qquad\qquad\qquad \text{for } n = p, p+1, \ldots, N-1 \\ \sum_{j=1}^{p} \tilde{C}_j \tilde{z}_j'^n \qquad \text{for } n = 0, 1, \ldots, p-1 \end{cases} \tag{20}$$

The first terms of both equations in (20) relate to the homogeneous solution of differential equation (1) and imply free oscillation. This term is necessary if $\tilde{x}_n$ is not zero when $n \le p-1$. The amplitude of the term $\tilde{C}_j$ can be estimated by fitting the data to eq. (20). The second and the third terms in the first equation of (20) together relate to the inhomogeneous solution of eq. (1). These terms imply forced oscillation.

2.7 Advantages of the excitation Sompi method

The present method has three advantages: (1) the method estimates both the eigen coefficients of the system and the excitation sequence mostly simultaneously; (2) the excitation sequence does not have any statistical constraints and is able to have a wide variety of characteristics; (3) the parameter estimation method is constructed to be robust for practical use: parameters with small error can be estimated even if the model assumptions are not fully satisfied.

The first advantage is derived from eqs (6) and (19). When we solve a set of linear equations with two variables, we first eliminate one variable and determine the other. Then, we determine the first eliminated variable. In spite of the two-step procedure, both variables are theoretically determined simultaneously. The present method is similar to this problem. We first eliminate parameter **B** associated with the excitation from eq. (6), and then estimate **A**. Next, we estimate the excitation sequence. For this estimation, we use eq. (19), which is an approximated relation, instead of eq. (2), which is precise. Hence, the simultaneous estimation of the eigen coefficients and the excitation is not completely achieved. However, this mostly simultaneous estimation is much more advanced than the previous methods, which can estimate either the eigen coefficients or the excitation sequence, or can estimate them both iteratively. This advantage implies that the parameters estimated by the present method have a smaller bias than those estimated by the previous methods, which require given or initial parameters.

The second advantage is clear from eq. (4). As can be seen from this treatment of the model, the basis set $\tilde{\varphi}_{n,j}$ does not have any statistical constraints. Of course, the selection of the set itself is a constraint, although various sets can be selected as the data warrant. Hence, flexibility in the expression of the excitation sequence is high. We also demonstrate this advantage in the next section.

The last advantage is derived from criterion (ii′). In a practical problem, a difference exists between the model system and the actual system. Most of the pre-existing methods do not take into account this difference and evaluate estimated parameters using statistical criteria, such as Akaike's information criterion (AIC), Akaike's Bayesian information criterion (ABIC), and so on (Akaike 1973, 1980). Our criterion contrasts with those methods: it takes into account a prediction error that does not obey the ideal statistical distribution, thus making the method robust. Hence, the practicability of the present method is higher than that of the pre-existing methods.

There is another, secondary, merit derived from criterion (ii′). The criterion makes parameter estimation possible without recovery of the output sequence. This reduces the computational load compared with the algorithm as previously described in papers II and III.

3 SYNTHETIC TEST

In this section, we present the results of a synthetic test to confirm the capability of the present method. Considering the application of the method to polar motion, we first summarized the features of

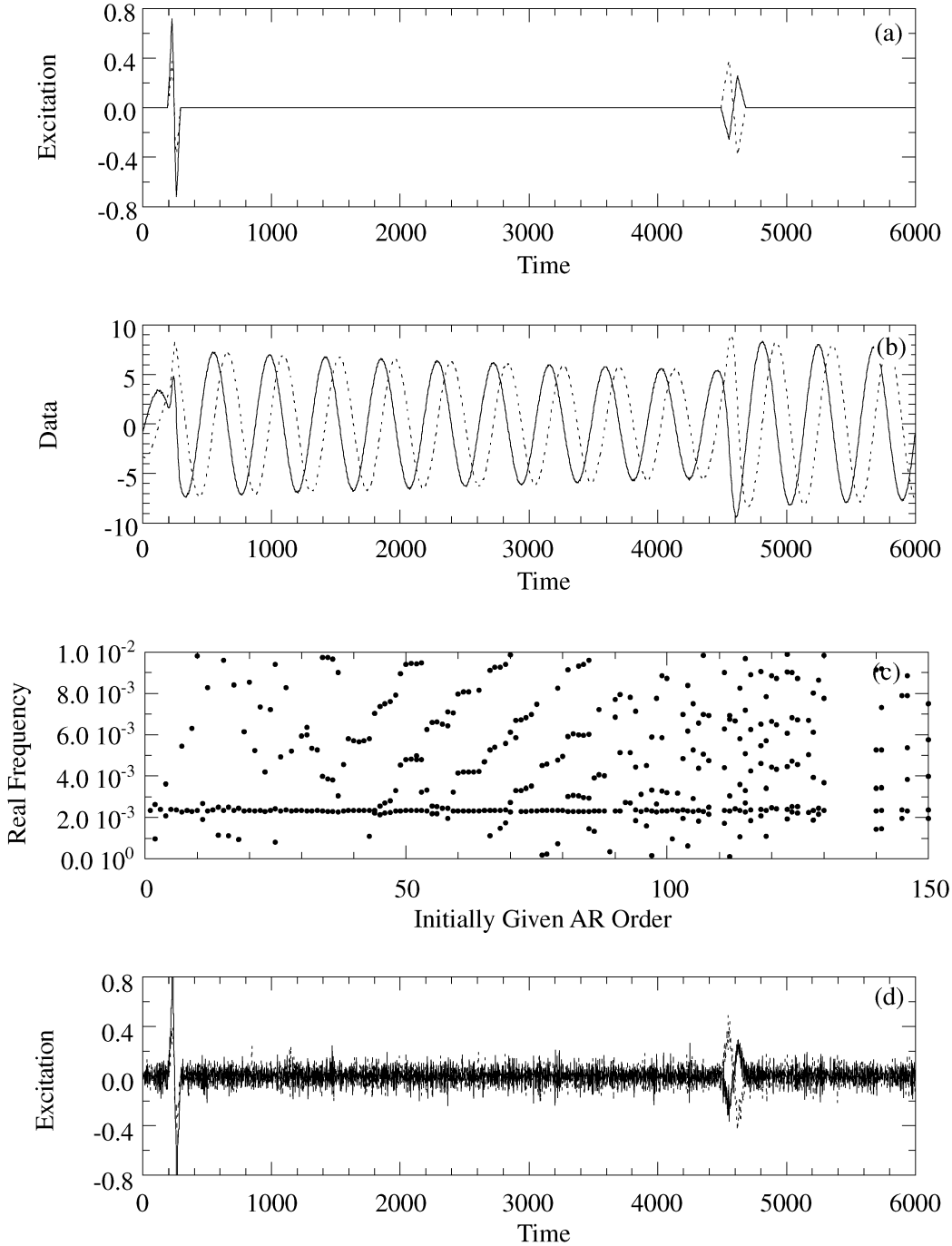

Figure 1. The results of the analysis of a test data set synthesized from an event-based excitation: (a) given excitation sequence, (b) synthesized data sequence, (c) estimated real frequencies with all initially given AR orders, and (d) estimated excitation sequence. A solid line and a broken line respectively indicate the first and the second components.

polar motion. Then we synthesized four data sets that have features similar to those of polar motion and analysed them.

3.1 Polar motion

When induced rotational changes are small, the displacement of the Earth's instantaneous rotation pole ω is approximated by the Liouville equation:

$$\frac{i}{\sigma_0}\frac{d\mathbf{m}(t)}{dt} \times \mathbf{m}(t) = \boldsymbol{\psi}(t) \tag{21}$$

In eq. (21), the complex dimensionless quantity **m** indicates the rotation pole within the fixed reference frame of a rotating body (e.g. Munk & MacDonald 1960; Lambeck 1980). The eigenfrequency of the equation, σ_0 is the frequency of the Chandler wobble. The observed real part of the eigenfrequency is about 2.30×10^{-3} cpd, as shown in Table 1, and Q is observed to be roughly anywhere from several tens to a thousand. The excitation term of the equation, the complex quantity $\boldsymbol{\psi}(t)$, is called the excitation function.

Polar motion is thought to be excited by various torques. Large contributions from an atmospheric torque and the ocean have been

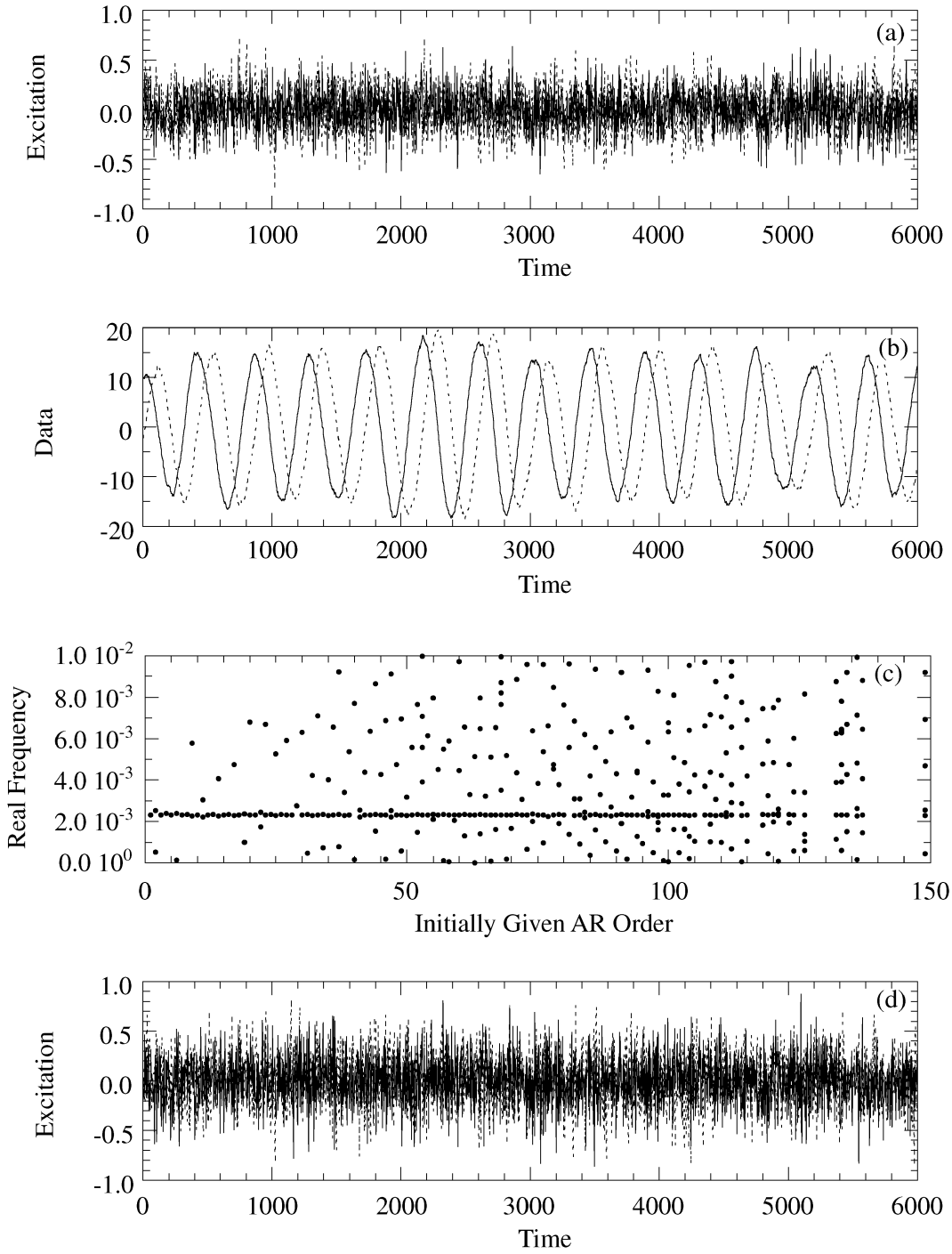

Figure 2. The results of the analysis of a test data set synthesized from random excitation.

reported in recent studies (Gross & Lindqwister 1992; Chao 1993; Rio & Cazenave 1994; Gross 2000). These excitations are found in polar motion on a timescale shorter than a few years and may have random phase and seasonal varying amplitudes. The core–mantle coupling may excite polar motion because of the high coherence between the decadal secular component of polar motion and the geomagnetic field induced in the core (Yokoyama 1993). There also may be event-based excitation. A large phase change was observed in the motion of the mean pole from 1920 to 1940 (Lambeck 1980). Event-based excitations caused by earthquakes and plate motion have also been proposed (Souriau & Cazenave 1985; Gross 1986; Alfonsi *et al.* 1997).

Polar motion is affected by excitation torque with various frequencies. Because of the wide range of timescales of the excitation torques described above, polar motion also has a wide variety of timescales: seasonal variation, the Chandler wobble, decadal variation, and longer term trends. In all cases, the motion is described with the same dynamic equation, and feedback of polar motion to the excitation torques is considered to be small. Accordingly, the dynamic equation (21) is regarded as linear. The system parameter of

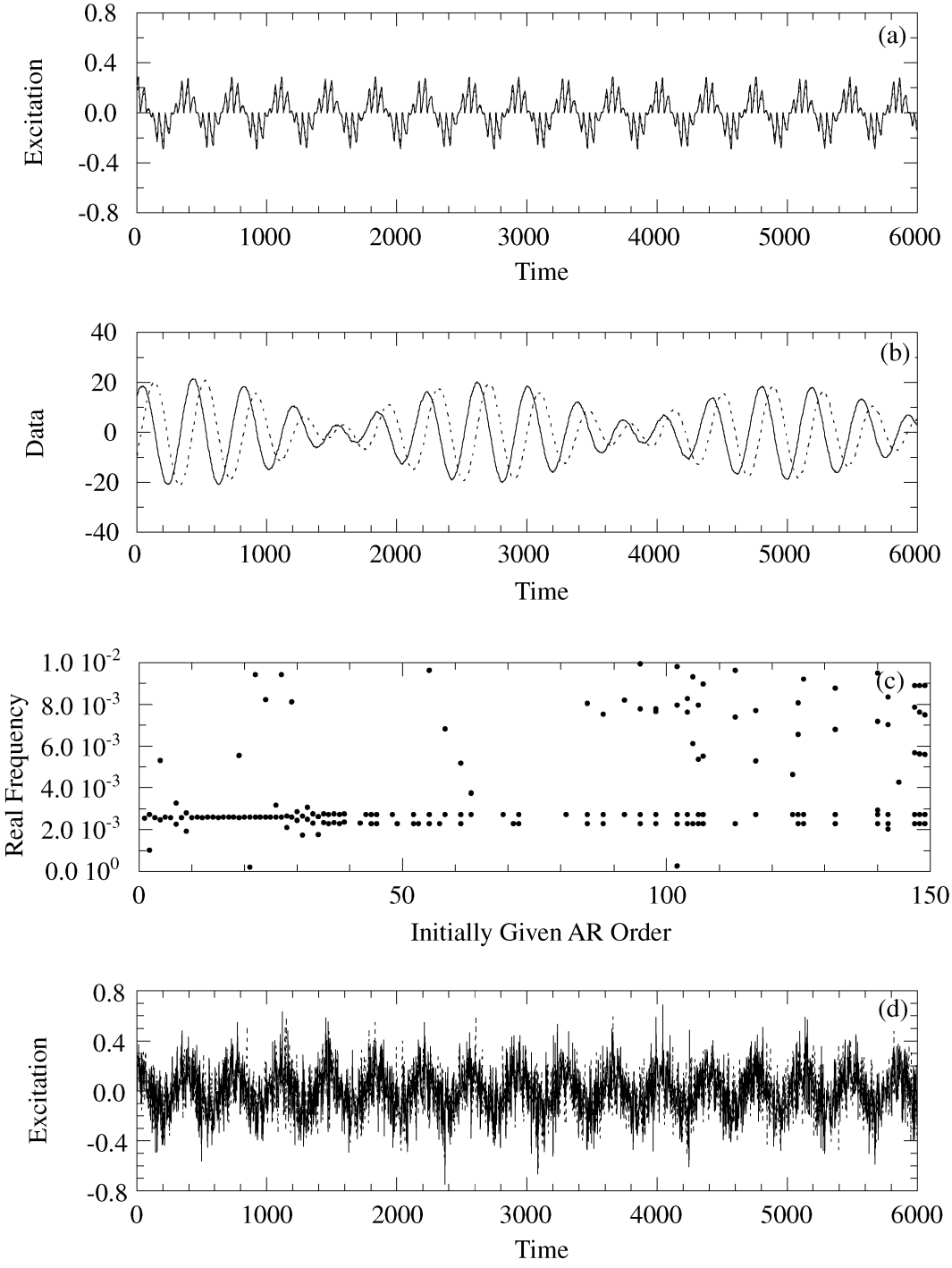

Figure 3. The results of the analysis of a test data set synthesized from periodic excitation.

the equation, the Chandler frequency, is regarded as time-invariant, because the mantle system on the short timescale discussed in this paper is time-invariant. Thus, the dynamic equation of polar motion is regarded as linear and time-invariant. Accordingly, it is described by the model of the present method, and both the Chandler frequency and the excitation function can be extracted using this method.

When we use the present method, we can use the following five kinds of information based on the above-mentioned features of polar motion.

(1) Polar motion has a single eigenfrequency because it obeys eq. (21). This indicates that the true AR order of the analysis model is one.

(2) On the basis of eq. (21), polar motion has a counter-clockwise rotation. That is, the real part of the eigenfrequency is positive.

(3) Although the eigenfrequency estimated by previous studies might include bias, its real part is roughly 2.30×10^{-3} cpd.

(4) The amplitude of the free oscillation never increases because of the law of energy conservation. That is, the sign of the imaginary

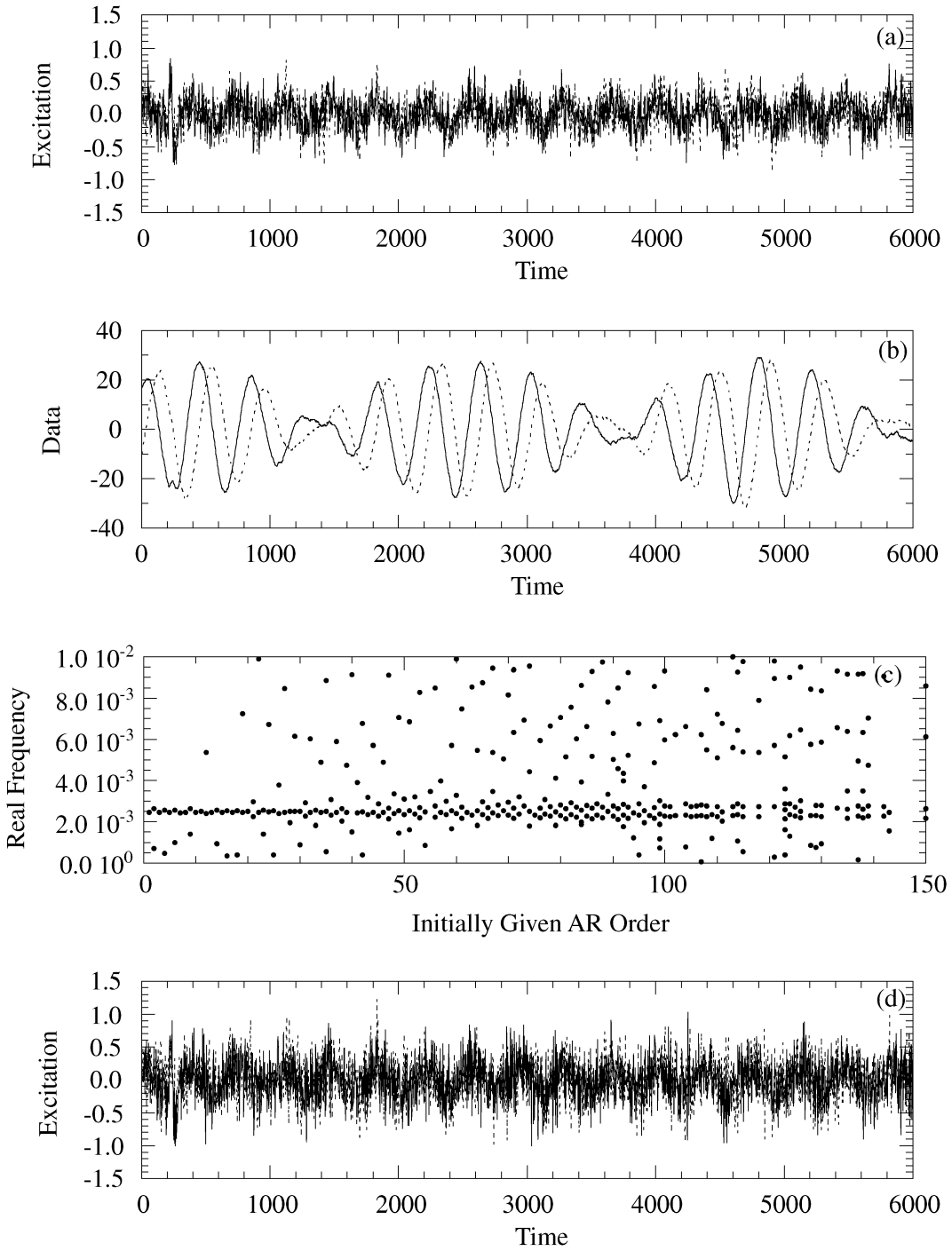

Figure 4. The results of the analysis of a test data set synthesized from the combined excitations.

part of the eigenfrequency, which corresponds to attenuation, is positive or zero.

(5) Various torques or combinations of torques are thought to excite polar motion.

3.2 Synthetic data

We created four data sets for numerical tests. The data sets were synthesized from excitation sequences and a common complex eigenfrequency. The first data set was synthesized from the event-based excitation shown in Fig. 1(a). The excitation sequence shows two events: one with width 32 (96 on the scale) at time 192 and one with width 64 (192 on the scale) at time 4488. The excitation of the second data set shown in Fig. 2(a) is a random sequence, and that of the third data set shown in Fig. 3(a) displays amplitude modulation with a period of 365. The excitation of the last data set is the sum of the first three excitations. This excitation sequence is shown in Fig. 4(a). We used an eigenfrequency of $2.300 \times 10^{-3} + 1.150 \times 10^{-5}$ i ($Q = 100$) to synthesize the four data sets. This value was taken from the previous studies as shown in Table 1. The synthesized sequences are shown in Figs 1(b)–4(b).

When we synthesized the data sets, we did not consider trends longer than several years. When considering the application of the method in the next section, we used a data length of 6000 days and a sampling interval of 3 days. That is, the number of data points is 2000. We added 40 dB of white noise, assuming a data precision greater than three significant figures.

3.3 Analysis of synthetic data

We analysed the four data sets using the *a priori* information mentioned above. Among the five kinds of information, (2) and (4) were used before selection of a preferred eigenfrequency to exclude improper frequencies. Information (1) and (3) was then used to select a preferred eigenfrequency: we selected only the one frequency closest to 2.30×10^{-3} cpd. Information (5) was used when we prepared

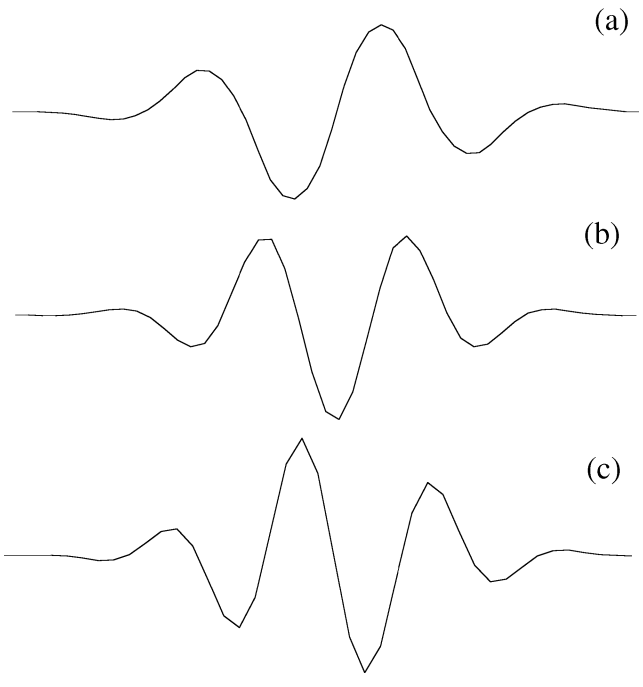

Figure 5. Functions of the candidate basis sets: (a) spline-3, (b) spline-4, and (c) spline-5.

Table 2. Candidate basis sets.

Basis set	Function width	Width (physical scale)
spl332	Spline-3	32 (96 days)
spl364	Spline-3	64 (192 days)
spl3128	Spline-3	128 (384 days)
spl432	Spline-4	32 (96 days)
spl464	Spline-4	64 (192 days)
spl4128	Spline-4	128 (384 days)
spl532	Spline-5	32 (96 days)
spl564	Spline-5	64 (192 days)
spl5128	Spline-5	128 (384 days)

candidate basis sets: we prepared basis sets able to describe the characteristics of the candidate excitations.

The candidate basis sets were created from spline wavelets of degree 3, 4 and 5 as shown in Fig. 5 (e.g. Chui 1992). By changing the degree and width of the spline wavelets, we can describe a wide variety of event-based, random and periodic excitation sequences. Then we created the basis sets using spline wavelets of three different degrees and with widths of 32, 64 and 128. That is, we prepared nine candidate basis sets as shown in Table 2. Because we did not consider longer-term trends, the maximum width of the wavelets is 128, which corresponds to 384 days on the physical scale. For short scales, wavelets with widths shorter than 32 might be necessary to describe a random excitation. However, short-scale wavelets increase the number of the basis and consequently increase the computational load. Hence, we described small-scale variations with higher degree spline wavelets instead of by using small-scale wavelets.

We first analysed the time-series synthesized from the event-based excitation shown in Fig. 1. Using the nine candidate basis sets and setting the initially given AR order $p = 1, 2, \ldots, 150$,we estimated frequencies. The estimated frequencies with all initially given AR orders and with the basis set spl432 are shown in Fig. 1(c). In this figure, the frequencies of negative real parts and negative imaginary parts were excluded on the basis of information (2) and (4). The remaining frequencies showed a stable frequency against initially given AR orders larger than 20. This stability was obtained also in the cases of the other candidate basis sets. Then we estimated the mean value of the stable frequency for $p = 20, 21, \ldots, 70$. The result is shown in Table 3. The scattering of the complex frequency was calculated from eq. (16), and the errors of the real and imaginary parts were respectively determined from the standard deviation of each part. Among the nine candidate basis sets, set spl432 showed the least scattering. Hence, we adopted the estimated parameters of that basis set. The estimated excitation sequence is shown in Fig. 1(d). Recovered data sequence is visually indistinguishable from the analysed sequence.

Next, we analysed the time-series synthesized from the random excitation shown in Fig. 2. In this case, we obtained a stable frequency with initially given AR orders higher than 10. Then we set $p = 10, 11, \ldots, 60$ and estimated the eigenfrequencies shown in Table 4. Basis set spl364 gave the best result, and we adopted the estimated value of that basis set.

The data set of the periodic excitation shown in Fig. 3 was also analysed. In this case, an apparently stable frequency appears with low initially given AR orders, then it splits into two stable frequencies with higher orders. This indicates that the two different frequencies could not be resolved with the low orders due to a large error as mentioned in Section 2.2. Then we set $p = 40, 41, \ldots, 90$, which is a range of resolved frequencies. Among the two stable

Table 3. Analysis results for event-based excitation.

Basis	Real frequency	Imaginary frequency	Scattering	RMS error
spl332	$(2.336 \pm 0.039) \times 10^{-3}$	$(6.237 \pm 28.376) \times 10^{-5}$	2.864×10^{-4}	2.307×10^{-1}
spl364	$(2.332 \pm 0.046) \times 10^{-3}$	$(1.250 \pm 2.185) \times 10^{-4}$	2.232×10^{-4}	2.740×10^{-1}
spl3128	$(2.340 \pm 0.018) \times 10^{-3}$	$(3.341 \pm 24.550) \times 10^{-5}$	2.461×10^{-4}	1.975×10^{-1}
spl432	$(2.329 \pm 0.031) \times 10^{-3}$	$(2.315 \pm 7.844) \times 10^{-5}$	8.429×10^{-5}	1.861×10^{-1}
spl464	$(2.338 \pm 0.029) \times 10^{-3}$	$(3.090 \pm 17.358) \times 10^{-5}$	1.760×10^{-4}	1.940×10^{-1}
spl4128	$(2.339 \pm 0.032) \times 10^{-3}$	$(1.627 \pm 3.275) \times 10^{-4}$	3.291×10^{-4}	2.872×10^{-1}
spl532	$(2.325 \pm 0.014) \times 10^{-3}$	$(5.842 \pm 44.918) \times 10^{-5}$	4.494×10^{-4}	2.265×10^{-1}
spl564	$(2.338 \pm 0.035) \times 10^{-3}$	$(6.546 \pm 31.691) \times 10^{-4}$	3.189×10^{-4}	2.342×10^{-1}
spl5128	$(2.338 \pm 0.027) \times 10^{-3}$	$(5.865 \pm 37.126) \times 10^{-5}$	3.723×10^{-4}	2.270×10^{-1}

Table 4. Analysis results for random excitation.

Basis	Real frequency	Imaginary frequency	Scattering	RMS error
spl332	$(2.320 \pm 0.015) \times 10^{-3}$	$(2.801 \pm 9.569) \times 10^{-5}$	9.690×10^{-5}	4.177×10^{-1}
spl364	$(2.320 \pm 0.019) \times 10^{-3}$	$(1.260 \pm 5.109) \times 10^{-5}$	5.442×10^{-5}	3.831×10^{-1}
spl3128	$(2.319 \pm 0.022) \times 10^{-3}$	$(1.625 \pm 8.701) \times 10^{-5}$	8.969×10^{-5}	3.890×10^{-1}
spl432	$(2.320 \pm 0.019) \times 10^{-3}$	$(1.555 \pm 6.486) \times 10^{-5}$	6.770×10^{-5}	3.879×10^{-1}
spl464	$(2.321 \pm 0.019) \times 10^{-3}$	$(1.818 \pm 8.933) \times 10^{-5}$	9.130×10^{-5}	3.936×10^{-1}
spl4128	$(2.320 \pm 0.025) \times 10^{-3}$	$(2.448 \pm 9.035) \times 10^{-5}$	9.380×10^{-5}	4.082×10^{-1}
spl532	$(2.318 \pm 0.025) \times 10^{-3}$	$(4.529 \pm 22.349) \times 10^{-5}$	2.248×10^{-4}	4.688×10^{-1}
spl564	$(2.320 \pm 0.021) \times 10^{-3}$	$(3.239 \pm 9.803) \times 10^{-5}$	1.002×10^{-4}	4.302×10^{-1}
spl5128	$(2.321 \pm 0.020) \times 10^{-3}$	$(3.756 \pm 17.244) \times 10^{-5}$	1.736×10^{-4}	4.459×10^{-1}

Table 5. Analysis results for periodic excitation.

Basis	Real frequency	Imaginary frequency	Scattering	RMS error
spl332	$(2.301 \pm 0.001) \times 10^{-3}$	$(1.139 \pm 0.353) \times 10^{-5}$	3.600×10^{-6}	6.344×10^{-1}
spl364	$(2.303 \pm 0.007) \times 10^{-3}$	$(1.290 \pm 0.118) \times 10^{-5}$	7.015×10^{-6}	6.336×10^{-1}
spl3128	$(2.301 \pm 0.001) \times 10^{-3}$	$(1.058 \pm 0.154) \times 10^{-5}$	1.727×10^{-6}	6.347×10^{-1}
spl432	$(2.303 \pm 0.008) \times 10^{-3}$	$(1.165 \pm 0.356) \times 10^{-5}$	8.316×10^{-6}	6.339×10^{-1}
spl464	$(2.303 \pm 0.010) \times 10^{-3}$	$(1.141 \pm 0.330) \times 10^{-5}$	1.067×10^{-5}	6.340×10^{-1}
spl4128	$(2.302 \pm 0.003) \times 10^{-3}$	$(1.132 \pm 0.371) \times 10^{-5}$	4.775×10^{-6}	6.342×10^{-1}
spl532	$(2.304 \pm 0.009) \times 10^{-3}$	$(1.221 \pm 0.324) \times 10^{-5}$	9.716×10^{-6}	6.334×10^{-1}
spl564	$(2.303 \pm 0.008) \times 10^{-3}$	$(1.155 \pm 0.112) \times 10^{-5}$	7.998×10^{-6}	6.339×10^{-1}
spl5128	$(2.303 \pm 0.007) \times 10^{-3}$	$(1.152 \pm 0.191) \times 10^{-5}$	7.569×10^{-6}	6.339×10^{-1}

Table 6. Analysis results for combined excitation.

Basis	Real frequency	Imaginary frequency	Scattering	RMS error
spl332	$(2.218 \pm 0.210) \times 10^{-3}$	$(3.801 \pm 8.648) \times 10^{-5}$	2.269×10^{-4}	9.104×10^{-1}
spl364	$(2.221 \pm 0.172) \times 10^{-3}$	$(3.351 \pm 7.397) \times 10^{-5}$	1.874×10^{-4}	9.067×10^{-1}
spl3128	$(2.221 \pm 0.105) \times 10^{-3}$	$(4.633 \pm 11.595) \times 10^{-5}$	1.564×10^{-4}	9.030×10^{-1}
spl432	$(2.201 \pm 0.205) \times 10^{-3}$	$(2.691 \pm 2.036) \times 10^{-5}$	2.057×10^{-4}	9.523×10^{-1}
spl464	$(2.218 \pm 0.196) \times 10^{-3}$	$(5.728 \pm 14.622) \times 10^{-5}$	2.446×10^{-4}	9.065×10^{-1}
spl4128	$(2.220 \pm 0.196) \times 10^{-3}$	$(4.195 \pm 8.008) \times 10^{-5}$	2.113×10^{-4}	9.055×10^{-1}
spl532	$(2.262 \pm 0.096) \times 10^{-3}$	$(3.437 \pm 5.241) \times 10^{-5}$	1.090×10^{-4}	8.130×10^{-1}
spl564	$(2.206 \pm 0.257) \times 10^{-3}$	$(4.288 \pm 6.836) \times 10^{-5}$	2.660×10^{-4}	9.324×10^{-1}
spl5128	$(2.208 \pm 0.231) \times 10^{-3}$	$(3.927 \pm 6.329) \times 10^{-5}$	2.397×10^{-4}	9.319×10^{-1}

frequencies, one of the frequencies is the eigenfrequency and the other is the excitation frequency. When the excitation sequence is periodic, it cannot be distinguished from the system eigenfrequency because the basis of the AR system is a complex exponential function. However, we fortunately have information (1) and (3) in this case, so we can select a frequency close to 2.30×10^{-3} cpd and calculated the mean frequencies as shown in Table 5. In this case, the preferred parameters were estimated using basis set spl3128.

The last time-series synthesized from the combined excitations, shown in Fig. 4, was also analysed. In this case, we have two stable frequencies, as in the third case, with initially given AR orders higher than 80. Then we set $p = 80, 81, \ldots, 130$ and obtained the result shown in Table 6. The parameters finally adopted were estimated using the basis set spl532.

We summarize the results of the four cases in Fig. 6. In all cases, two significant figures of the estimated real frequencies correspond, and the true values lie within their error bars. With respect to the imaginary part of the eigenfrequency, the estimated values in all cases correspond to within one order of magnitude, and the true value is also within their error bars. Because the absolute value of the real part is much larger than that of the imaginary part, the error of the imaginary part is larger than that of the real part. The estimated excitation sequence also corresponds well to the given sequence in each case.

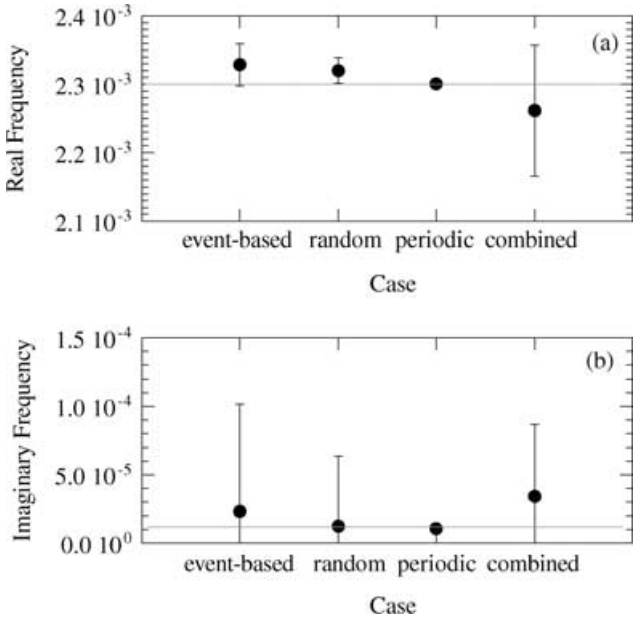

Figure 6. Estimated (a) real and (b) imaginary frequencies from the four test data sets. A gray line indicates the true value.

Both a complex eigenfrequency and an excitation sequence close to the given values were thus estimated. This successful result indicates that the present method works even with model selection error caused by the selection of the basis set. The ability of the method to describe a variety of excitation sequences is also shown by the result. Because we succeeded in our analyses of examples similar to polar motion, the results of the analysis of actual polar motion performed in the next section will be reliable.

4 ANALYSIS OF POLAR MOTION

In this section, we apply the present method to actual polar motion data. We used the polar motion data of SPACE95 (Gross 1996) shown in Fig. 7(a). The data duration is from 1976 to 1996. The sampling interval is 3 days, and the number of data points is 2355. Although SPACE95 reports not m but the location of $\mathbf{p} = (PMX - iPMY)$ the celestial ephemeris pole (CEP), the dynamic equation of $\mathbf{p}$ is the same as that of m :

$$\frac{i}{\sigma_0}\frac{d\mathbf{p}(t)}{dt} + \mathbf{p}(t) = \boldsymbol{\chi}(t) \tag{22}$$

Hence, we can apply the present method to the data in a similar way as in the previous section. Note that the estimated excitation sequence in this case will be $-i\sigma_0\boldsymbol{\chi}(t)$.

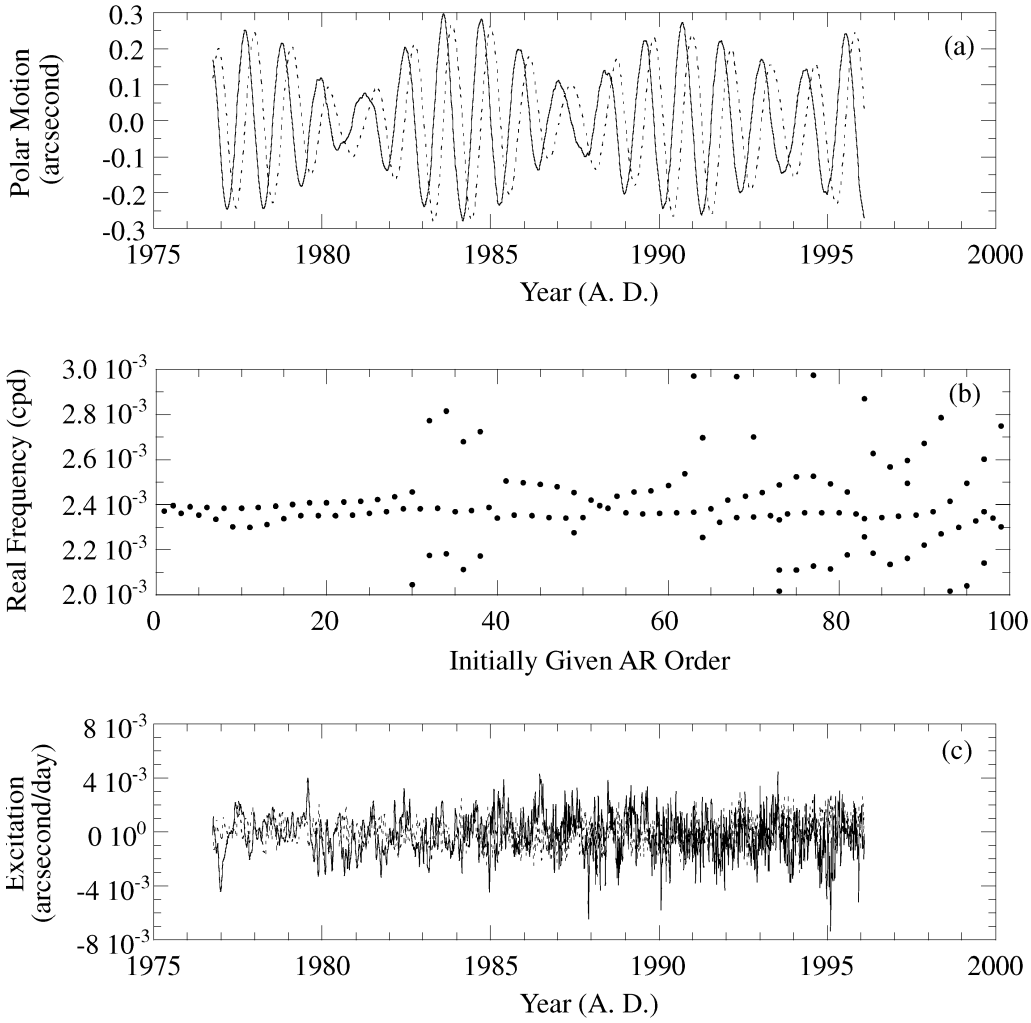

Figure 7. The results of the analysis of polar motion: (a) analysed data, SPACE95, (b) estimated real frequencies with all initially given AR orders, and (c) estimated excitation sequence. A solid line and a broken line respectively indicate x- and y-components.

Table 7. Polar motion analysis results.

Basis	Real frequency (cpd)	Imaginary frequency (cpd)	Scattering (cpd)	RMS error (arc sec)
spl332	$(2.361 \pm 0.038) \times 10^{-3}$	$(6.694 \pm 10.826) \times 10^{-6}$	3.965×10^{-5}	6.718×10^{-3}
spl364	$(2.362 \pm 0.040) \times 10^{-3}$	$(6.454 \pm 5.320) \times 10^{-6}$	4.019×10^{-5}	6.803×10^{-3}
spl3128	$(2.359 \pm 0.032) \times 10^{-3}$	$(1.322 \pm 2.457) \times 10^{-5}$	4.038×10^{-5}	6.633×10^{-3}
spl432	$(2.361 \pm 0.042) \times 10^{-3}$	$(7.342 \pm 7.179) \times 10^{-6}$	4.256×10^{-5}	6.712×10^{-3}
spl464	$(2.362 \pm 0.036) \times 10^{-3}$	$(6.966 \pm 6.385) \times 10^{-6}$	3.705×10^{-5}	6.798×10^{-3}
spl4128	$(2.363 \pm 0.045) \times 10^{-3}$	$(8.637 \pm 4.622) \times 10^{-6}$	4.571×10^{-5}	6.814×10^{-3}
spl532	$(2.362 \pm 0.038) \times 10^{-3}$	$(7.194 \pm 4.022) \times 10^{-6}$	3.773×10^{-5}	6.806×10^{-3}
spl564	$(2.361 \pm 0.038) \times 10^{-3}$	$(7.541 \pm 6.005) \times 10^{-6}$	3.869×10^{-5}	6.755×10^{-3}
spl5128	$(2.362 \pm 0.032) \times 10^{-3}$	$(8.262 \pm 4.850) \times 10^{-6}$	3.224×10^{-5}	6.801×10^{-3}

Setting the initially given AR order $p = 1, 2, \ldots, 100$ and using the nine candidate basis sets in Table 2, we estimated frequencies. The result in the case of spl5128 is shown in Fig. 7(b). In all basis sets, two stable frequencies appear for p higher than 20. Then we calculated the mean frequency for $p = 20, 21, \ldots, 70$.

The results are shown in Table 7. Real frequencies estimated by the different basis sets agree within three significant figures. Imaginary frequencies correspond within one order of magnitude. In summary, the results given by different basis sets are mostly the same. This indicates the robustness of the parameter estimation method: parameters with a small error are successfully estimated in spite of the model selection error that results from mis-selection of the basis set.

Although there is not a clear difference among the results of the nine basis sets, we finally adopted the result of spl5128, because its scattering of the frequency is the smallest. The estimated real part of the frequency $(2.362 \pm 0.032) \times 10^{-3}$ cpd and imaginary part is $(8.262 \pm 4.850) \times 10^{-6}$. This is equivalent to a Chandler period of 423 days (418–429 days) and a Q of 143 (90–346). The estimated excitation sequence is shown in Fig. 7(c). Seasonal and shorter variations are visible in the sequence, and large excitations are recognized at 1977, 1979, 1985, 1988, 1990, 1995, and 1996.

Such features are well distinguishable in wavelet space (e.g. Combes *et al.* 1989). Fig. 8 shows wavelet transformed excitation sequence by a spline-5 wavelet, which is a function of the adopted basis set. In Fig. 8, both x- and y-components have similar characteristics although the amplitude of the y-component is smaller than that of the x-component.

The strongest signal in the wavelet-transformed excitation sequence is seen on a scale of approximately 2048 days. Signs and intervals of the signals are not periodic, but the mean interval is 661 days. Because this scale is biannual, it is considered to relate to the quasi-biennial oscillation (QBO) as suggested by Rio & Cazenave (1994).

The strongest secondary signal was seen on a scale of approximately 512 days. There are pairs of positive and negative signals. On a scale of approximately 256 days, there are signal peaks that appear at an interval half that of the signal at around 512 days. The periodicity of the two kinds of signals were determined by Fourier analysis to be 368 and 184 days. Hence, the signals are seasonal variations as suggested by Chao (1993).

On a scale shorter than the seasonal variation, no typical signal pattern is observed. A Fourier spectrum with this scale in Fig. 9 shows a broad spectrum, which implies coloured random excitation as discussed in Chao (1993).

Besides the typical scales mentioned above, signal patterns with a wide scale band are also seen in Fig. 8. In particular, there are strong patterns at 1979, 1988, and 1990 as also seen in Fig. 7(c). The large excitation at 1985 is not recognized in Fig. 8 as a wide band signal. These wide band patterns indicate large and rapid changes in the excitation. Although the physical cause is not clear, these are considered to be event-based excitations.

The estimated excitation sequence thus includes biannual quasi-periodic, annual and semiannual periodic, random, and event-based variations. Hence, we conclude that a compound excitation sequence, as well as a complex eigenfrequency, was successfully extracted with the present method.

5 SUMMARY AND DISCUSSION

We developed a practical excitation Sompi method. This method is based on a model of a linear time-invariant dynamic equation and is able to estimate both the system parameters and the excitation sequence mostly simultaneously. Its parameter estimation method is robust and works well even when the model assumptions are not fully satisfied; it estimates parameters with small errors.

A remarkable difference between the present and previous methods was demonstrated by analyzing four synthetic data sets. The present method succeeded in the estimation of proper parameters, even when the given data sets were created from excitation sequences with extremely different features. This contrasts with the previous methods, which can estimate only excitations with limited characteristics and which may have a large estimation bias.

We also analysed polar motion data utilizing the advantages of the present method. As a result, we obtained an eigenfrequency with a value different from those previously obtained. The estimated real eigenfrequency was $2.36 \times 10^{-3} (2.33 \times 10^{-3} - 2.39 \times 10^{-3})$ cpd and Q was 143 (90–346). On the other hand, the real frequency of the previous studies shown in Table 1 was about 2.30×10^{-3} and Q was from several tens to a thousand.

Because the previous methods cannot estimate the eigenfrequency and excitation together, and because they do not take into account model selection error, the estimated values may include a large bias. In particular, they tend to estimate a smaller real eigenfrequency, because the frequency of the variation seems to be smaller when the excitation positively acts. This is thought to be why the previous methods estimated smaller eigenfrequencies. On the other hand, we took into account both the excitation and the model selection error, so we succeeded in estimating an eigenfrequency whose value is much closer to the true value.

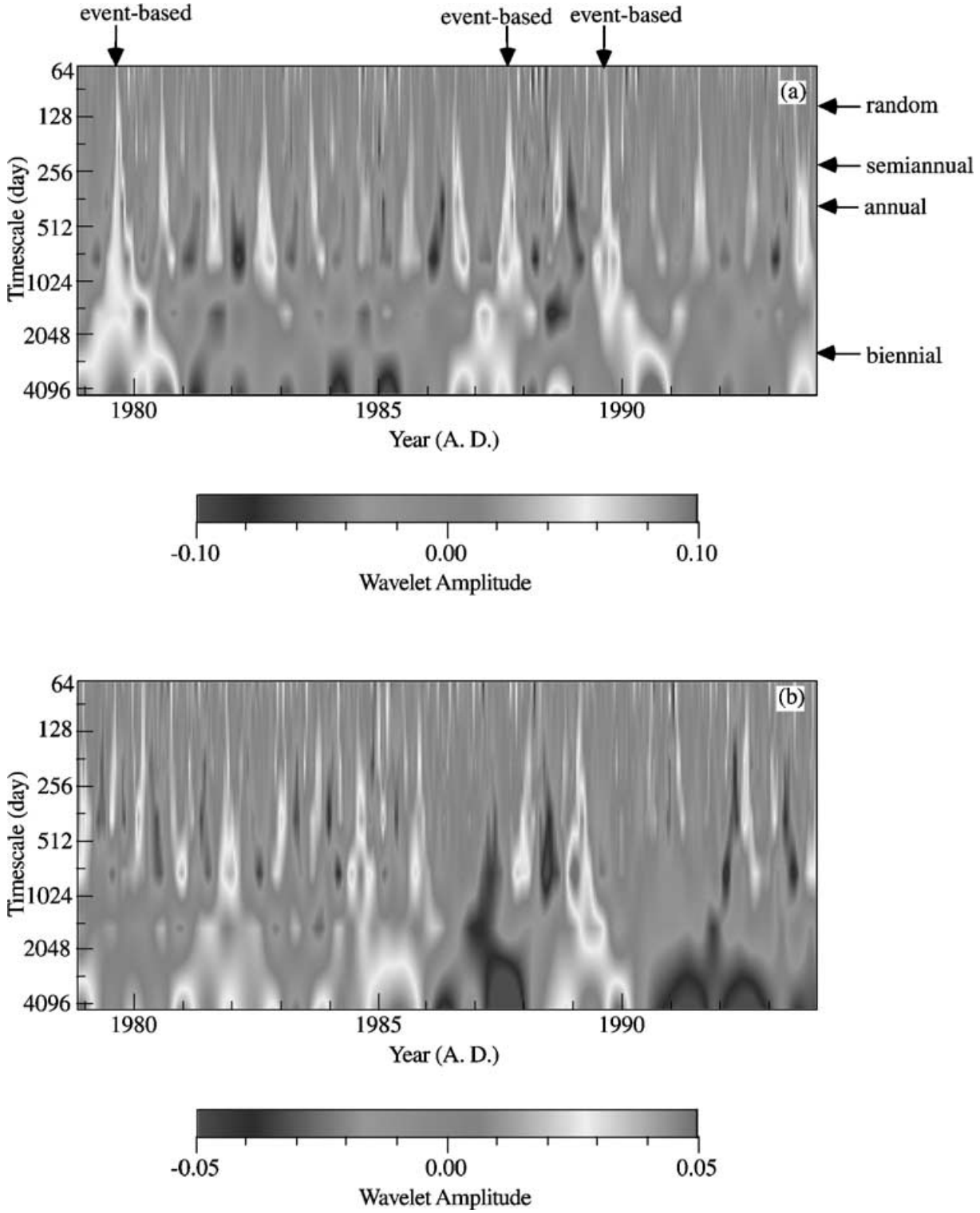

Figure 8. Wavelet-transformed excitation sequences of the (a) x-component and (b) y-component.

With respect to Q, a similar bias may be generated by the previous methods. For the same reason, they tend to estimate a large Q. However, the previously estimated Q had a large error region, and the value estimated by the present method falls within that region. For this reason, the difference between the previous studies and this study is not clear. Nevertheless, the region of Q estimated in this study is relatively narrow, and the value is not too large. From this point of view, we succeeded in restricting Q.

We have thus shown that the present method is useful for the practical analysis of physical data. This method can be applied to other

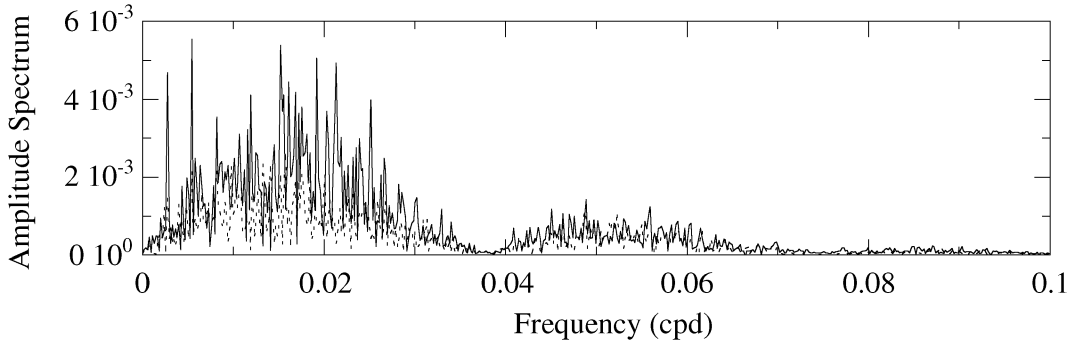

Figure 9. Amplitude spectrum of the wavelet component on a scale shorter than seasonal variation. The solid and broken lines respectively indicate the x- and y-components.

kinds of data whose dynamic processes are linear and time-invariant. Hence, the method will be a powerful tool to extract physical information about various geophysical phenomena.

REFERENCES

Akaike, H., 1973. Information theory and an extension of the maximum likelihood principle, in *Second International Symposium on Information Theory,* pp. 267–281, eds Petrov, B.N. & Czaki, F., Akademiai Kiado, Budapest.

Akaike, H., 1980. Likelihood and the Bayes procedure, in *Bayesian Statistics,* pp. 143–166, eds Bernardo, J.M., DeGroot, M.H., Lindley, D.V. & Smith, A.F.M., Univ. Press, Valencia.

Alfonsi, L., Piersanti, A. & Spada, G., 1997. Did the 1977 Sumba earthquake excite the Chandler wobble?, *Earth planet. Sci. Lett.,* **153,** 287–292.

Box, G.E.P. & Pierce, D.A., 1970. Distribution of residual autocorrelations in autoregressive integrated moving average time-series model, *J. Am. statist. Assoc.,* **65,** 1509–1526.

Chao, B.F., 1983. Autoregressive harmonic analysis of the Earth's polar motion homogeneous international latitude service data, *J. geophys. Res.,* **88,** 10 299–10 307.

Chao, B.F., 1993. Excitation of Earth's polar motion by atmospheric angular momentum variations, 1980–1990, *Geophys. Res. Lett.,* **20,** 253–256.

Chui, C.K., 1992. An Introduction to Wavelets, Academic, Boston.

Combes, J.M., Grossmann, A. & Tchamitchian, Ph. 1989. Wavelets, Time Frequency Methods and Phase Space, Springer-Verlag, Berlin.

Dembo, A. & Zeitouni, O., 1988. Maximum a posteriori estimation of time-varying ARMA processes from noisy observations, *IEEE Trans. Signal Processing,* **36,** 471–476.

Fowler, C.M., 1990. The Solid Earth, Cambridge University, Cambridge.

Furuya, M. & Chao, B.F., 1996. Estimation of period and Q of the Chandler wobble, *Geophys. J. Int.,* **127,** 693–702.

Grenier, Y. & Omnes-Chevalier, M.C., 1988. Autoregressive models with time-dependent log area ratios, *IEEE Trans. Signal Processing,* **36,** 1602–1612.

Grewal, M.S. & Andrews, A.P., 1993. Kalman Filtering—Theory and Practice, Prentice-Hall, Englewood Cliffs.

Gross, R.S., 1986. The influence of earthquakes on the Chandler wobble during 1977–1983, *Geophys. J. R. astr. Soc.,* **85,** 161–177.

Gross, R.S., 1996. A Combination of EOP measurements: SPACE95. Summerized in: 1995 IERS Annual Report, Obs de Paris, Paris, II11.

Gross, R.S., 2000. The excitation of the Chandler wobble, *Geophys. Res. Lett.,* **27,** 2329–2332.

Gross, R.S. & Lindqwister, U.J., 1992. Atmospheric excitation of polar motion during the GIG '91 measurement campaign, *Geophys. Res. Lett.,* **19,** 849–852.

Huber, P.J., 1981. Robust Statistics, Wiley, New York.

Jeffreys, H., 1968. The variation of latitude, *Mon. Not. R. astr. Soc.,* **141,** 255–268.

Kalman, R.E. & Bucy, R.S., 1961. New results in linear filtering and prediction theory, *Trans. ASME, J. Basic Eng.,* **83D,** 95–108.

Kanai, H., Chubashi, N., Kido, K., Koiwa, Y., Takagi, T., Kikuchi, J. & Takishima, T., 1992. A new approach to time dependent AR modelling of signals and its application to analysis of the fourth heart sound, *IEEE Trans. Signal Processing,* **40,** 1198–1205.

Kassam, S.A. & Poor, H.V., 1985. Robust techniques in signal processing: a survey, *Proc. IEEE,* **73,** 433–481.

Kay, S.M. & Marple, S.L., 1981. Spectrum analysis—a modern perspective, *Proc. IEEE,* **69,** 1380–1419.

Kosek, W. & Kolaczek, B., 1997. Semi-Chandler and semiannual oscillations of polar motion, *Geophys. Res. Lett.,* **24,** 2235–2238.

Kuehne. J., Wilson, C.R. & Johnson, S., 1996. Estimates of the Chandler wobble frequency and Q, *J. geophys. Res.,* **101,** 13 573–13 579.

Lambeck, K., 1980. The Earth's Variable Rotation,pp. 30–61, Cambridge University, Cambridge.

Moritz, H. & Mueller, I.I., 1988. Earth Rotation, Ungar Publishing, New York.

Munk, W.H. & MacDonald, G.J.F., 1960. The Rotation of the Earth, Cambridge University, New York.

Nagpal, K.M. & Khargonechker, P.P., 1991. Filtering and smoothing in an setting, *IEEE Trans. Automat. Contr.,* **36,** 152–166.

Ooe, M., 1978. An optimal complex ARMA model for the Chandler wobble, *Geophys. J. R. astr. Soc.,* **53,** 445–457.

Oppenheim, A.V. & Schafer, R.W., 1999. Discrete Time Signal Processing,pp. 693–774, Prentice Hall, Upper Saddle River.

Preisig, J.R., 1992. Polar motion, atmospheric angular momentum excitation and earthquakes—correlations and significance, *Geophys. J. Int.,* **108,** 161–178.

Rio, R.A. & Cazenave, A., 1994. Interannual variations in the Earth's polar motion for 1963–1991: comparison with atmospheric angular momentum over 1980–1991, *Geophys. Res. Lett.,* **21,** 2361–2364.

Shaked, U. & Theodor, Y., 1992. Optimal estimation: a tutorial, *Proc. 31st IEEE Conf. Decision and Control,* 2278–2286.

Souriau, A. & Cazenave, A., 1985. Re-evaluation of the seismic excitation of the Chandler wobble from recent data, *Earth planet. Sci. Lett.,* **75,** 410–416.

Tukey, J.W., 1974. Introduction to Today's data analysis, in *Proceedings of the conference on critical evaluation of chemical and physical structural information,* pp. 3–14, eds Lide, Jr. D.R. & Paul, M.A., National Academy of Sciences, Washington.

Wilson, C.R. & Vincente, R.O., 1980. An analysis of the homogeneous ILS polar motion series, *Geophys. J. R. astr. Soc.,* **62,** 605–616.

Wilson, C.R. & Vincente, R.O., 1990. Maximum likelihood estimates of polar motion parameters, in *Variations in Earth Rotation,* pp. 151–155, eds McCarthy, D.D. & Carter, W.E., AGU, Washington.

Yokoyama, Y., 1993. Thirty year variations in the earth rotation and the geomagnetic Gauss coefficients, *Geophys. Res. Lett.,* **20,** 2957–2960.

Yokoyama, Y., 2000. A new method of AR order estimation, *Proc. Digital Signal Processing,* 197–202 (in Japanese).

Yokoyama, Y., Kumazawa, M., Imanishi, Y. & Mikami, N., 1997. A new method of non-stationary time-series analysis based on inhomogeneous AR equation, *IEEE Trans. Signal Processing,* **45,** 2130–2136.

Yokoyama, Y., Kumazawa, M. & Mikami, N., 1999. Parameter estimation of inhomogeneous AR model expanded with unknown basis, *IEICE Trans. Fundamentals,* **E82-A,** 1582–1587.

Yokoyama, Y., Kumazawa, M. & Mikami, N., 2000. Estimation of the AR order of an inhomogeneous AR model with input expanded by a set of basis, *IEICE Trans. Fundamentals,* **E83-A,** 551–557.